Adv Polym Sci
DOI:10.1007/12_2010_67

Processes of Ordered Structure Formation in Polypeptide Thin Film Solutions

Ioan Botiz, Helmut Schlaad, and Günter Reiter

Abstract An experimental study is presented on the hierarchical assembly of α-helical block copolymers polystyrene–poly(γ-benzyl-L-glutamate) into anisotropic ordered structures. We transformed thin solid films into solutions through exposure to solvent vapor and studied the nucleation and growth of ordered three-dimensional structures in such solutions, with emphasis on the dependence of these processes on supersaturation with respect to the solubility limit. Interestingly, polymer solubility could be significantly influenced via variation of humidity in the surrounding gas phase. It is concluded that the interfacial tension between the ordered structures and the solution increased with humidity. The same effect was observed for other protic non-solvents in the surrounding gas phase and is attributed to a complexation of poly(γ-benzyl-L-glutamate) by protic non-solvent molecules (via hydrogen-bonding interactions). This change of polymer solubility was demonstrated to be reversible by addition or removal of small amounts of protic non-solvent in the surrounding gas phase. At a constant polymer concentration, ordered ellipsoidal structures could be dissolved by removing water or methanol present in the solution. Such structures formed once again when water or methanol was reintroduced via the vapor phase.

Keywords Humidity · Hydrogen bonding · Macromolecular self-assembly · Nucleation · Solvent effects · Supersaturation

I. Botiz
Center for Nanoscale Materials, Argonne National Laboratory, 9700 South Cass Avenue, Argonne, IL 60439 USA
e-mail: ibotiz@anl.gov

H. Schlaad
Colloid Chemistry, Max Planck Institute of Colloids and Interfaces, Research Campus Golm, 14424 Potsdam, Germany
e-mail: Helmut.Schlaad@mpikg.mpg.de

G. Reiter (✉)
Physikalisches Institut, Universität Freiburg, 79104 Freiburg, Germany
e-mail: guenter.reiter@physik.uni-freiburg.de

Contents

1 Introduction

Many biological and synthetic macromolecular systems can self-assemble in a hierarchical way, and may even have the ability to undergo a third, fourth, etc. ordering process [1–13]. Structured polymeric materials often exhibit remarkably diverse assemblies of building blocks, frequently arranged in a hierarchical way on multiple length-scales that range from nanometers to macroscopic sizes. As one sub-group of such polymers, rod–coil block copolymers are attracting significant interest for the development of functional surfaces based on novel self-assembled polymeric structures. Rod–coil block copolymers consist of a rigid block, for instance a polypeptide that has internal order and a well-defined shape, and an amorphous block with random (statistical) conformations. Due to the combination of stiff parts that partially interact via directional forces, and a highly flexible coil part, it is expected that such systems are able to generate structures of various shapes, possibly providing interesting properties. Ordered structures on surfaces based on such systems may, for example, be used for purposes such as the development of novel sensors or actuators.

In this context, investigation of the processes of structure formation in thin films of polypeptide block copolymer solutions is the first step towards control of the ways such polymers follow during ordering. By exposure to solvent vapor, thin films can be transformed into solutions while keeping the geometry of a thin film. Combined with microscopy, this approach allows the study of the nucleation and growth of ordered solid structures in solutions by varying systematically and within a single sample the concentration of polymer (c_p), from a "critical concentration" ($c_{critical}$ or polymer solubility) up to very concentrated solutions [14].

The present study focuses mainly on diblock copolymers and star block copolymers based on a coiled polystyrene (PS) part and an α-helical poly(γ-benzyl-L-glutamate) (PBLGlu) part. However, for the purpose of comparison, simpler systems like homopolymers were also investigated. Thin films were analyzed mainly by optical microscopy (OM) and atomic force microscopy (AFM). The central focus was on the process of nucleation and its dependence on environmental parameters like humidity.

2 Experimental

2.1 Polymers

The primary sample investigated was an AB_n heteroarm star block copolymer, denoted PS_{63}–$(PBLGlu_{37})_8$, consisting of eight poly(γ-benzyl-L-glutamate) (PBLGlu = B) blocks on average, attached to the backbone of a single amorphous polystyrene (PS = A) block (see the chemical structure in Fig. 1a). A schematic representation of this polymer is given in Fig. 1b. Figure 1c shows one possible arrangement of the helices in an ordered state. Details about the synthesis and the characterization of this polymer are given elsewhere (see the appendix of [14]). The α-helical secondary structure of PBLGlu – the result of intramolecular hydrogen-bonding interactions – makes PBLGlu a rigid macrodipole with a high overall permanent dipole moment (theoretically 3.5 Debye per repeat unit) caused by the organization of the individual dipoles of the carbonyl groups of the peptide bond such that they point along the helix axis [15–17].

For the purpose of comparison, we also studied a homopolymer of PBLGlu and two diblock copolymers having the same PS block (52 repeat units) and differing PBLGlu blocks (31 and 104 repeat units) [18].

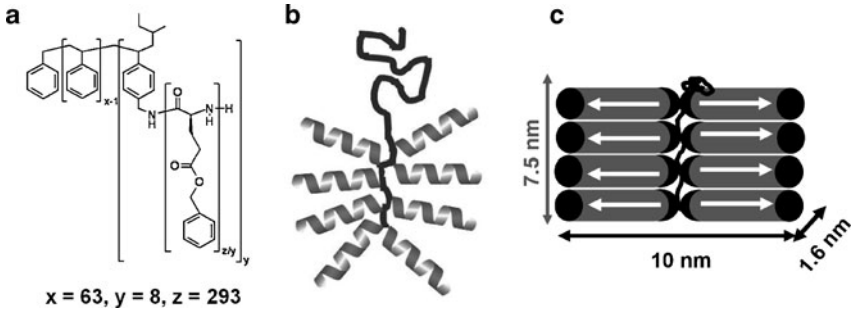

Fig. 1 (**a**) Chemical structure and (**b**) representation of PS_{63}–$(PBLGlu_{37})_8$ heteroarm star block copolymer. (**c**) 3D representation of a possible arrangement of the α-helical PBLGlu block in the ordered state. The *arrows* indicate the dipole moment of PBLGlu

2.2 Preparation and Observation of Thin Film Solutions

Thin solid films of PS_{63}–$(PBLGlu_{37})_8$ with an average thickness of a few tens of nanometres (as determined by ellipsometry) were obtained by spin-casting of chloroform ($CHCl_3$) polymer solutions onto hydrophilic UV/ozone-cleaned silicon wafers.

Increasing molecular mobility by heating the polymers was not possible because the polymers decomposed before melting. The morphology of none of the spin-coated solid films changed over time, even when the films were heated to 200°C for 60 min. The films were therefore exposed to solvent vapor and turned into concentrated polymer solutions, in order to enable the polymer chains to move, which, in turn, facilitated the structure formation processes. Finally, after structure formation, the dry samples were characterized in detail by OM (Leitz, Metallux 3, Germany) and AFM (Dimension 3000, Nanoscope III, Veeco, USA) in the tapping mode (TM-AFM).

Polished silicon substrates were used because of their excellent reflective properties, which, coupled with an interference phenomenon due to reflected light coming from the film–air and the substrate–film interfaces, gave us the possibility to use OM for our studies. Swelling the spin-coated films in such reflection geometry in a saturated solvent atmosphere allowed us to study processes of structure formation in solutions in real time and direct space by OM. Moreover, using OM for such thin films allowed the variation and direct evaluation of the polymer concentration (c_p) by determining the thickness of the swollen films from the interference colors.

Interference colors were calibrated in order to obtain values of the (solution) film thickness. First, several films with different thicknesses (in steps of about 20 nm between 5 and 200 nm in thickness) were spin-coated from solutions of increasing polymer concentration. The thickness of each film was measured in the dry state by ellipsometry. In parallel, the interference color of each film was determined by OM. Consequently, we obtained a series of distinct interference colors together with the corresponding film thicknesses. The thickness of films having an interference color in between these calibrated colors was interpolated, allowing continuous determination of the thickness of a "film-solution" during swelling and de-swelling. The calibration films used are shown in Fig. 2a. Taking into account that the colors depend somewhat on the setup of the optical microscope (light intensity, sensitivity of the CCD detector), the refractive index (which slightly depends on c_P), and the subjective judgment of the experimenter, we obtained an absolute thickness resolution of about 10 nm. However, relative changes during swelling/de-swelling and during structure formation could be observed with a higher precision of a few nanometers.

2.3 "Equilibrium" and "Off-Equilibrium" Experiments

By exposing thin films to solvent vapor, the swelling of thin films could be done using two different approaches: either by condensation of solvent vapor onto the cooled film surface (denoted as "off-equilibrium" experiments) or by exposure of

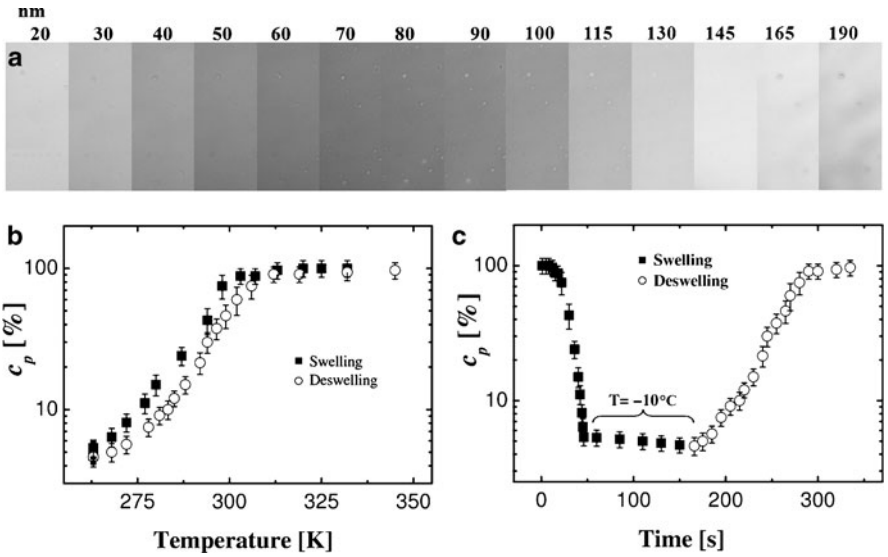

Fig. 2 Swelling and de-swelling of thin films: (**a**) calibration series used in this study (color versus film thickness, ranging from 20 to 190 nm); (**b**) evolution of the polymer concentration during swelling and de-swelling as a function of film temperature; and (**c**) corresponding temporal evolution of the polymer concentration (c_p) during swelling and de-swelling (using chloroform vapor)

thin films to chloroform under conditions without any gradients in temperature (denoted as thermodynamic "equilibrium" experiments). Generally, condensation is controlled by the temperature T_C to which the film surface was cooled below the temperature T_A of the ambient solvent vapor phase, i.e., by the undercooling $\Delta T = T_A - T_C$.

It is important to emphasize that during experiments in ambient air, the polymer molecules were in contact with water molecules from the air. In order to obtain dry air conditions, we used phosphorus pentoxide (P_2O_5) as a desiccant.

To expose thin solid films to solvent vapor, a homebuilt sample chamber was used. It contained two compartments connected via an opening that could be closed when needed. Using two compartments (one for solvent and one for the sample) allowed cooling or heating of both the sample and the solvent independently by using separate Peltier heating/cooling stages for each compartment. The limited temperature range (between about -10 and 65°C) imposed by the Peltier elements did not allow us to use solvents with high boiling points and low volatility [for example *N,N*-dimethylformamide (DMF) with a boiling point of 153°C]. However, solvents such as $CHCl_3$ or tetrahydrofuran (THF) were well suited.

When performing off-equilibrium experiments, solvent (heated to 50°C in the solvent compartment) was sent into the neighboring compartment, where the sample was initially kept at 35°C. The walls of the sample compartment, however, were not heated. Thus, the sample chamber always stayed approximately at room temperature, with the exception of the sample it contained. After a few minutes, the

sample was in equilibrium with solvent vapor at the temperature of the sample compartment. Under such conditions, not much solvent could be found within the film because its temperature was above the temperature of the vapor phase, which was mainly determined by the temperature of the walls of the sample chamber. Decreasing the sample temperature to a few degrees below the temperature of the surrounding vapor phase led to solvent condensation onto the film and allowed for its swelling. It should be noted that at the same time as condensation of solvent molecules onto the films, small amounts of water from the surrounding air within the chamber were also condensed onto the film, except when precautions (P_2O_5) against humidity were taken.

2.4 Determining the Concentration of Thin Film Solutions

By using an optical microscope, solvent condensation could be followed in real time and direct space via the change of the interference colors of the film. As the amount of polymer in the film stayed constant (this quantity is proportional to the thickness of the dry spin-coated film), a change in film thickness was directly related to the amount of solvent incorporated into the film, i.e., corresponded to swelling by solvent. From the interference colors the thickness (h) of the swollen film could be deduced. The initial film thickness (h_0) was determined by ellipsometry. Accordingly, the polymer concentration c_P in the solution of the swollen film was determined by:

$$c_P = h_0/h \tag{1}$$

In Fig. 2b, a typical temperature-dependence of c_P is shown for a film during swelling/deswelling and for a constant temperature of the solvent reservoir. The corresponding evolution in time is shown in Fig. 2c. Keeping the film at a constant and low temperature led to a slow but steady decrease of the c_P due to continuously condensing solvent molecules (see Fig. 2c for the lowest c_P). Thus, for experiments of long durations, c_P was kept roughly constant by continuously increasing slightly the sample temperature.

Similarly to swelling the film via solvent condensation (i.e., decreasing c_P), c_P could be augmented by increasing the sample temperature and thereby evaporating solvent from the film. A pronounced hysteresis in $c_P(T)$ was observed. At a given temperature, c_P differed between the decreasing and the increasing temperature branch (see Fig. 2b). Finally, at a time chosen to stop the experiment, the sample was dried completely by simply heating the film to relatively high temperatures, for example to 65°C.

In summary, one can distinguish three stages during exposure of thin films to solvent vapor: (1) swelling of films up to (low) c_P; (2) controlled de-swelling by partial evaporation of the solvent from the swollen films; and finally (3) complete drying of films.

3 Results and Discussions

3.1 Nucleation in Solution Films in Dry Air

In order to obtain high molecular mobility of polymers, films were swollen until c_P decreased to about 5%. At this concentration, the molecules were distributed homogeneously and the molecular mobility was high. As the viscosity of such an isotropic solution was comparatively low, surface tension was able to smooth the surface of the film quickly within seconds (heterogeneities in film thickness, as observed by OM on spin-coated films, disappeared). This smoothing process was taken as a clear indication for having reached the isotropic phase.

At c_P of about 5%, no changes in time were detectable by OM. The films stayed smooth for many hours. However, when c_p was increased to above 50%, the films started to exhibit local changes in thickness (the corresponding heterogeneities on the film surface could be observed directly under the optical microscope), which were related to the formation of ordered structures within the film. At such increased c_P, the average distance between neighboring molecules became small enough to allow for the formation of nuclei, which led to the growth of ordered structures. This process can be compared to undercooling a polymer melt, thus allowing for nucleation and growth of ordered solid structures. At present, it cannot be decided whether these ordered structures grew from an isotropic solution or from an already (pre)ordered liquid crystalline (LC) phase [19–32]. However, AFM measurements performed after drying the solution film did not indicate any order of the phase surrounding these grown structures.

Figure 3 presents a typical example, which demonstrates that OM is undeniably able to follow in situ both the exposure of films to solvent vapor (i.e. the formation of a solution film by solvent swelling) and the structure formation process. Figure 3a shows the smooth, homogeneous surface of an initially 50 ± 2 nm thick film that had been previously swollen in $CHCl_3$ vapor (using an off-equilibrium approach) up to a thickness of about 1 µm and was subsequently brought back to 95 ± 5 nm, i.e., to c_P of about $53 \pm 5\%$.

After reaching a polymer concentration of $53 \pm 5\%$, the film stayed homogeneous for about 20 min (see Fig. 3a). Later on, isolated "inhomogeneities" started to appear randomly within the film, as observed directly under the optical microscope (see Fig. 3b). Of course, OM has its limitations in resolution (the lateral resolution in this case is about 1 µm) and the optical contrast is typically weak. This contrast is generated mainly by variations in film thickness and to a minor extent by small differences in the refractive index between the solution and the solid phase. Fortunately, at a concentration of $c_P = 53 \pm 5\%$, the growth process was slow enough to be followed in real time. In addition, the nucleation density was low enough that individual objects were sufficiently separated so that they could be resolved by OM. Thus, structure formation could be clearly detected, starting after approximately 25 min at $53 \pm 5\%$ of polymer. After about 30 min, the surface was extensively covered with isolated objects (Fig. 3c). It is worth emphasizing that OM allowed us to

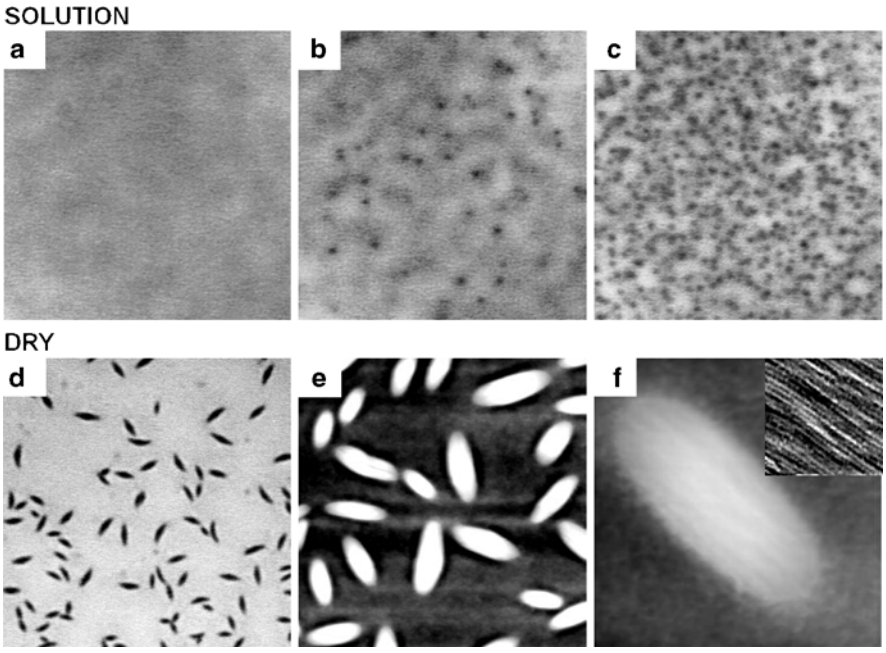

Fig. 3 (**a–d**) Series of OM and (**e**, **f**) AFM topography images showing the temporal evolution of a 50 ± 3 nm thick film at $c_p = 53 \pm 5\%$ after (**a**) 20, (**b**) 25, and (**c**) 30 min. (**d–f**) Final film morphology after total drying of the film. This film was spin-coated from chloroform solution and swollen under dry air conditions (P_2O_5) using chloroform vapor. The *inset* in (**f**) represents a phase AFM image magnified in a region on top of the ellipsoidal structure. The sizes of images are (**a–c**) 100×100, (**d**) 35×35, (**e**) 5×5, and (**f**) $0.8 \times 0.8\,\mu m^2$

verify that these structures already existed in solution and were not formed only at a later stage, for example during the drying of the film. After the rapid initial stage of their formation, these objects did not measurably increase in size, even for prolonged times of up to 1 day. This stop in growth can be attributed to the reduction of the concentration of the remaining solution below the critical concentration of supersaturation, due to extraction of the molecules forming the grown objects.

After 30 min at $53 \pm 5\%$ of polymer, the sample was dried and analyzed by OM and AFM. Isolated, randomly distributed ellipsoidal structures embedded in a surrounding film of low degree of order could be identified, as shown in Fig. 3d–e. A detailed morphology of such an ellipsoidal three-dimensional (3D) structure is shown in Fig. 3f. The inset of this figure shows the result of phase-contrast of TM-AFM, which allowed the detection of parallel straight stripes on top of the ellipsoidal structure. These stripes are spaced at an average characteristic distance of molecular dimension: 12 ± 3 nm, which is comparable to about twice the contour length of one block of $PBLGlu_{37}$ in the α-helix conformation. Intermolecular hydrogen bonding may act normal to the long axis of PBLGlu α-helices, forming long linear stacks of helices (showing as one stripe). This probably explains the existence of parallel straight stripes spaced at a molecular distance and homogeneously covering the whole surface of the grown objects.

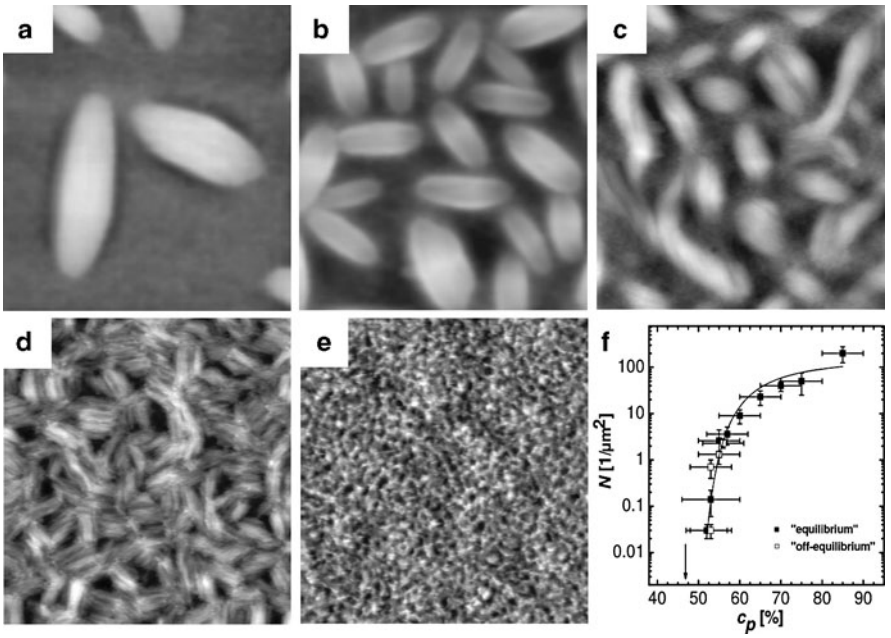

Fig. 4 Series of AFM topography images showing the morphology of 50 ± 3 nm thick films swollen at different c_p: (**a**) 53, (**b**) 55, (**c**) 57, (**d**) 65, and (**e**) 85%. The dependence of nucleation density N on c_p is shown in (**f**). Thin films were spin-coated from chloroform solution and swollen under dry air conditions (P_2O_5) using chloroform vapor. Note that for (**a**) and (**b**) off-equilibrium experiments were used, and on-equilibrium for (**c**), (**d**), and (**e**). The *arrow* in (**f**) indicates the $c_{critical}$ of $47 \pm 3\%$ (solubility in chloroform), below which no structures could be detected experimentally. The size of all images is $2.5 \times 2.5\,\mu m^2$

Figure 4 presents the experimentally determined dependence of the number density [33–36] $N(c_P)$ of ellipsoidal objects nucleated in thin films swollen in chloroform vapor to variable c_P (ranging from 53 up to 85% of polymer). N, the total number of structures per unit area, was determined by OM and/or AFM after complete drying of the films. These experiments were performed under dry air conditions. As can be seen in Fig. 4a–e, the number of ordered ellipsoidal structures increased with c_P. At the same time, the size of ordered ellipsoidal structures decreased. Figure 4f represents a summary of $N(c_P)$ for all experiments that were performed under dry air conditions. N increased with c_P (see Fig. 4f) because it is less difficult to form a nucleus at higher c_P when molecules are close to each other. However, at large numbers of nuclei per unit volume, the resulting ordered structures will rapidly meet each other (coalesce) during growth due to the short distance between the nucleation sites. Thus, the maximum size of these structures is always smaller than the average distance between the initial nucleation sites. Accordingly, the average size of the structures will be small (see Figs. 4d–e). In order to obtain bigger structures, c_P was decreased until only a few objects nucleated, which then could grow to larger sizes at high nucleation density (see Fig. 4a). Consequently,

in order to be able to employ OM as an observation tool, experiments focused on rather small c_P that were close to a critical concentration $c_{critical}$. Under such conditions, the formed structures could exceed the micrometer size. Interestingly, all films that were exposed at c_P lower than ca. 53% never showed any indication of nucleation during exposure to chloroform vapor, and no ordered structures were detectable after drying of these films. Thus, one may conclude that the solubility limit in chloroform (represented by $c_{critical}$) was slightly below 53%. An extrapolation of the $N(c_P)$ curve (Fig. 4f) to 10^{-8} objects per μm^2 (one object per cm^2, i.e., one object per surface of the whole film) yielded $c_{critical} = 47 \pm 3\%$ (refer to the black vertical arrow in Fig. 4f). In order to estimate the error bars for this value of $c_{critical}$, the uncertainty in determining the polymer concentration $\Delta c_p = \pm 5\%$ for each point of the $N(c_p)$ curve has to be taken into account. Two graphical extrapolations, using either the highest or lowest possible values given by Δc_P, to10^{-8} objects per μm^2 were made, yielding $\Delta c_{critical} = \pm 3\%$.

The line in Fig. 4f represents a fit to a theoretical description [35, 36] of the nucleation density as given by the following equation:

$$\ln N = \ln P - \frac{Q\beta\sigma^3 v^2}{(kT)^3} \cdot \frac{1}{[\ln(c_P/c_{critical})]^2} \tag{2}$$

Here, P is an intercept (its exact value depends on the details of the theoretical model chosen) representing the maximum possible number of nuclei for $c_P = 1$, Q characterizes the type of growth, σ represents the interfacial energy between nucleus and solution, β is a shape factor, v represents the volume of the monomeric species, k is the Boltzmann constant, and T is the absolute temperature.

3.2 Nucleation in Solution Films in Ambient Air

The ordering process was also studied under ambient air conditions, i.e., without P_2O_5 as desiccant to eliminate the humidity of the surrounding gas phase. Thus, during an off-equilibrium film-swelling process, some water molecules were also condensed when condensing solvent vapor onto the film surface, and during the equilibrium experiments, thin films were in contact with water molecules contained in surrounding gas phase.

As shown in Fig. 5, OM allowed the structure formation process to be followed in situ and in real time in thin film solutions. Figure 5a shows the smooth, homogeneous surface of an initially 30 ± 3 nm thick film that was initially swollen in chloroform vapor up to a thickness of about 600 nm and then brought back to 100 nm (i.e., at $c_P = 305\%$). At this concentration, the film surface was initially homogeneous (see Fig. 5a). However, it quickly became inhomogeneous due to the appearance of many individual objects protruding from the surrounding film. Structure formation could be clearly observed starting after approximately 6 min at $c_P = 30 \pm 5\%$ (see Fig. 5b). Again, OM allowed verification that these structures already existed in solution.

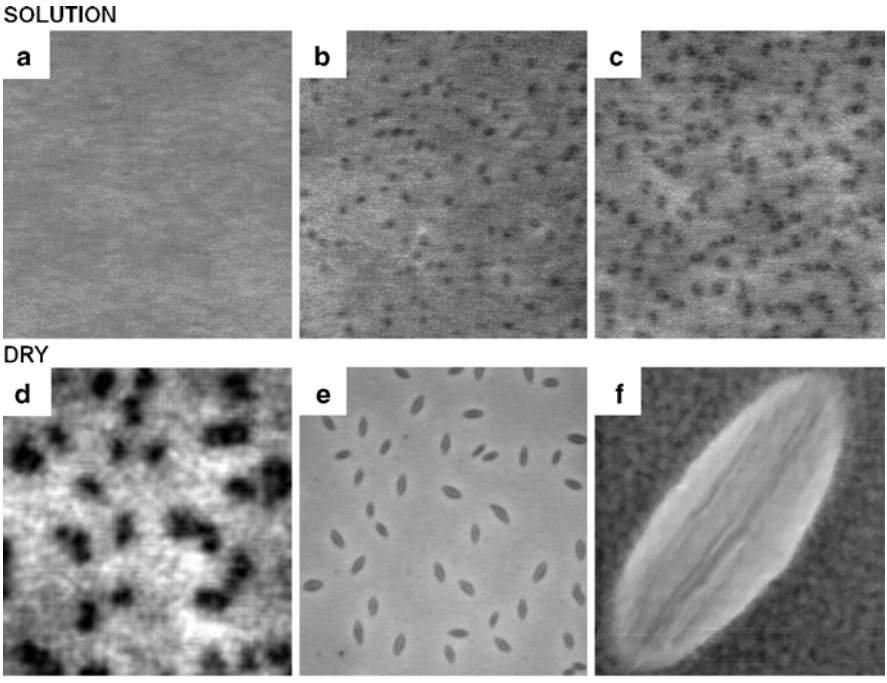

Fig. 5 (**a–e**) Series of OM and (**f**) AFM topography images showing the temporal evolution of a thin film during swelling: (**a**) after 10 s, (**b**) after 6 min, (**c**) after 60 min. (**d**) Magnification of (**c**). (**e**) Magnification of the dried film shown in (**f**). This film was spin-coated from tetrahydrofuran solution and swollen using chloroform vapor at $c_p = 30 \pm 5\%$. The sizes of the images are (**a–c**) 100×100, (**d**, **e**) 45×45, and (**f**) $2.5 \times 2.5\,\mu m^2$

After comparatively rapid formation, the resulting objects did not increase significantly in size, even after prolonged times (see Fig. 5c). It is supposed that the concentration of chains remaining in solution decreased below supersaturation. After 60 min at $c_P = 30 \pm 5\%$, the sample was rapidly dried and analyzed by OM and AFM. The observed isolated structures of ellipsoidal shape were embedded in a film with a low degree of order, as shown in Figs. 5e–f. Note that a magnified area of the still-swollen film (at $c_p = 30 \pm 5\%$) shown in Fig. 5d allowed the observation of protrusions, which corresponded to the ordered ellipsoidal structures shown in Fig. 5e. This was confirmed by subsequent AFM investigations after drying the film.

Systematic experiments revealed that under ambient air, ordered ellipsoidal structures could be obtained at c_P as low as 16–25%. Below c_P of 16–25%, no nucleation and growth of structures could be detected. This raises the question of why structures could be formed in ambient humid air at such low c_P? As demonstrated for dry air conditions, the concentration below which no structures could be nucleated was as high as 47%. Evidently, the only difference between both experiments is the presence of some water molecules in the surrounding gas phase.

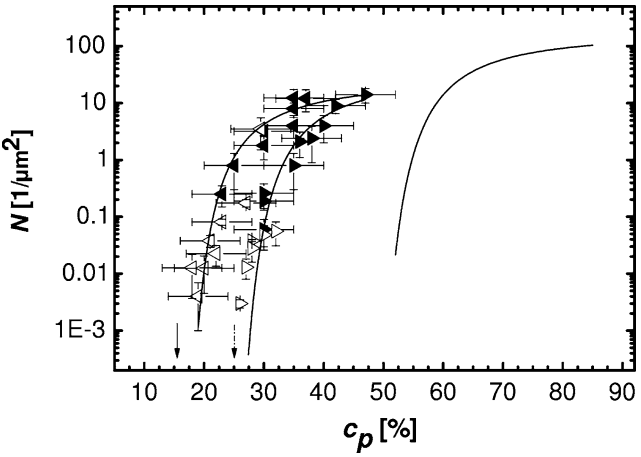

Fig. 6 Representation of nucleation density N versus polymer concentration c_P as determined from off-equilibrium (*filled symbols*) and equilibrium (*empty symbols*) experiments carried out under ambient conditions at low humidity (*right pointing triangles*) and at high humidity (*left pointing triangles*). The *dotted* and *solid arrows* indicate the experimental $c_{critical}$ (solubility in chloroform) of about $25 \pm 3\%$ and $16 \pm 2\%$ determined for less and more humid environments, respectively. Note that below these $c_{critical}$ no structures could be detected experimentally. The *lines* represent the theoretical fits obtained using (2). The isolated *line* at high c_P represents a fit for data points presented in Fig. 4f

It has to be concluded that humidity could lower $c_{critical}$. To rationally explore such a possibility, all results obtained under various ambient air conditions were sorted as a function of the humidity in the laboratory. Such separation allowed us to realize that results obtained in air of ca. 30% humidity ("sunny days") differed from results obtained under ca. 50% humidity ("rainy days") (see in Fig. 6 the right- and left-pointing triangles, respectively). As can be seen in Fig. 6, the two series led to different values of $c_{critical}$ of about $25 \pm 3\%$ and $16 \pm 2\%$, respectively, below which no structure formation was detectable. The lines in Fig. 6 represent fits to the data using the theoretical description of (2).

In 1984, Russo and Miller [37] showed that small amounts of water, which can be easily absorbed even from the atmosphere under normal ambient conditions, seriously alter the phase behavior and morphology of PBLGlu homopolymer solutions. This observation is also relevant for the present experiments. When swelling PBLGlu films in humid air, water molecules from the atmosphere obviously entered the polymer solution film. Based on the experiments presented above, it thus can be concluded that water (a non-solvent for the polymer system) facilitates ordering and structure formation, even at low polymer concentrations. In order to verify this statement, complementary experiments were performed on films prepared in air of 100% humidity. Under such conditions, a higher amount of water molecules was expected to condense on the film surface during the film-swelling process. Such conditions of water-saturated air were obtained by including a few droplets of water in the

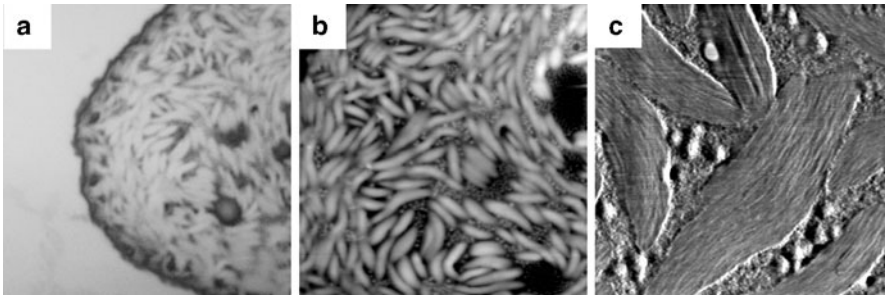

Fig. 7 OM (**a**) and TM-AFM (**b** topography, **c** phase) images showing the morphology of a film made of PS_{63}–$(PBLGlu_{37})_8$ and exposed to chloroform vapor at 100% humidity for 50 min at c_P of about 10–15%. Sizes of images are (**a**) 25×25, (**b**) 17.5×17.5, and (**c**) $3.5 \times 3.5\,\mu m^2$

sample chamber before the film-swelling process was started. At 100% humidity, a significantly larger amount of water molecules condensed on the film surface during the swelling process compared to the case of ambient air conditions (30–50% humidity).

In the corresponding experiments, 25 ± 2 nm thick films were exposed to chloroform vapor under off-equilibrium conditions. The subsequent OM and AFM investigations – performed after drying of the film – revealed (Fig. 7) that the resulting morphology consisted of ellipsoidal ordered structures. By comparing the details of the ellipsoidal structures shown if Fig. 7c with the ones obtained under ambient or dry air conditions, it can be concluded that the morphology is essentially unaffected by the presence of water, at least on the length-scales that are resolved by OM and AFM.

Results of systematic experiments performed for various concentrations of the solution films at 100% humidity are summarized in Fig. 8a (see the upward-pointing triangles). They prove that it was possible to form ellipsoidal ordered structures under 100% humidity conditions even at a very low c_P of about 3–5%. One can determine (by extrapolation) a $c_{critical}$ of about $0.5 \pm 0.4\%$, below which no structure formation will be possible. It should be noted that the way of determining the concentration introduces a large number of uncertainties, particularly for low values of c_P.

The lines in Fig. 8a represent the best fits to the experimental data based on (2). These fits contained three parameters: P, $Q\beta\sigma^3\nu^2/(kT)^3$ and $c_{critical}$. The fitted values of $c_{critical}$ were compared to those obtained by graphical extrapolation and are summarized in Table 1. As can be seen, the two sets of values are in reasonable agreement. In Fig. 8b, the fitted values for $Q^{1/3}\beta^{1/3}\sigma\nu^{2/3}/kT$ are presented as a function of humidity of the surrounding gas phase, with only the interfacial tension σ between ordered structures and the surrounding solution as a variable. This presentation clearly shows that σ varied with humidity: the greater the amount of water (a non-solvent for PBLGlu) in the surrounding gas phase, the higher the value of σ (see Fig. 8b). In Fig. 8c, we show that $Q^{1/3}\beta^{1/3}\sigma\nu^{2/3}/kT$ and $c_{critical}$ are also correlated and that σ varied inversely with $c_{critical}$: the lower was $c_{critical}$, the higher was σ.

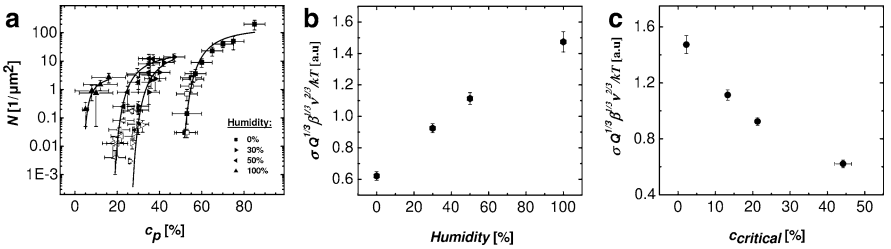

Fig. 8 (**a**) Representation of nucleation density N versus polymer concentration c_P as determined from off-equilibrium (*filled symbols*) and equilibrium (*empty symbols*) experiments carried out: in dry air (*squares*), at low humidity (*right pointing triangles*), at high humidity (*left pointing triangles*) and in water-vapor-saturated air (*upwards pointing triangles*). (**b**, **c**) Variation of interfacial tension σ between the solid ordered structures and solution. The interfacial tension σ increased with an increase in surrounding gas phase humidity (**b**), and with the decrease of polymer solubility c_{critical} (**c**)

Table 1 Comparison of c_{critical} values obtained both experimentally (by extrapolation) and by fitting according to (2), for different humidity conditions

Humidity (%)	Extrapolated c_{critical} (%)	Fitted c_{critical} (%)
0	47 ± 3	44.2 ± 2.3
30	25 ± 3	21.3 ± 2
50	16 ± 2	13.3 ± 2
100	0.5 ± 0.4	2.22 ± 1

3.3 Influence of Protic Non-Solvents on Nucleation in Thin Film Solutions

What could be the explanation for such dependence, knowing that water is not a solvent, neither for PBLGlu nor for PS? However, PBLGlu does offer several possible sites that can interact with water via hydrogen-bonding interactions (for example, the polar L-glutamate backbone and the polar ester group).

In the search for a tentative concept to explain the dependence of σ on humidity of the surrounding gas phase, one may assume that protic non-solvent (water) molecules form a complex with PBLG via hydrogen-bonding interactions. This complex is then expected to exhibit a lower solubility c_{critical}. Among the various possibilities for hydrogen bonding, the two hydrogen bonds of type C=O $\cdots$ H–O between the oxygen atom of the ester carbonyl group and hydrogen atom of water seem to be most favorable. The ester group is located at the exterior of the PBLGlu helix and is not otherwise involved in hydrogen bonding. The secondary amide groups of the PBLGlu backbone, on the other hand, are involved in intramolecular hydrogen bonding, stabilizing the α-helical conformation of PBLGlu, and are hidden inside the core of the helix. Other possibilities of hydrogen-bonding interactions (for example C–H $\cdots$ O–H) cannot be excluded, but will not be considered further.

If this concept is valid, it means that other non-solvents, with similar properties akin to water, should also be able to complex the PBLGlu and to modify its solubility. Furthermore, this concept implies that non-solvents without hydrogen-bonding capabilities should not be able to complex the polymer. If these conclusions were proven, they would represent strong support of our concept of polymer complexation.

In order to test the hypothesis, two series of off-equilibrium experiments were performed by exposing thin films to chloroform vapor mixed with small amounts of (1) methanol and (2) toluene. Methanol is a "strongly hydrogen-bonding" protic non-solvent that can form hydrogen bonds with the polymer. Toluene, although it is a good solvent for PS, does not dissolve PBLGlu (at room temperature). It is an aprotic "poorly hydrogen-bonding" non-solvent [38] for PBLGlu and does not strongly interact with PBLGlu, and certainly does not form hydrogen bonds. Small amounts of methanol or toluene molecules were added to the surrounding gas phase by placing several droplets of these liquids in the sample chamber before swelling of the film. Humidity was avoided either by flushing the sample chamber with nitrogen before the start of the experiment (in the case of methanol, as methanol is absorbed by P_2O_5) or by using P_2O_5 (in the case of toluene).

An example of such off-equilibrium experiments in the presence of methanol will be described. Polypeptide films of 40 ± 3 nm thickness were exposed to chloroform vapor mixed with a small amount of methanol molecules and swollen up to $c_P = 5 \pm 2\%$, which was subsequently increased in two steps to c_P of $30 \pm 5\%$ for 30 min and then to c_P of $45 \pm 5\%$ for 2 min before the film was finally dried.

As can be seen in Fig. 9a–b, ellipsoidal ordered structures were obtained at low c_P of $30 \pm 5\%$. In addition, many smaller ordered structures formed at the higher polymer concentration $(45 \pm 5\%)$. It has to be noted that both concentrations were lower than the critical concentration found in experiments performed in dry air without the addition of small amounts of a protic solvent like methanol. This experiment, together with previous and with additional experiments, proved that ordered ellipsoidal morphology does not depend on the type of non-solvent (water or methanol). In Fig. 9c we have summarized the corresponding results. With respect to results obtained in dry air, we observed that methanol did decrease c_{critical}, and toluene did not affect c_{critical}. Accordingly, these results strongly suggest that complexation of PBLGlu by protic non-solvents via hydrogen-bonding interactions causes a decrease in solubility.

3.4 Reversible Influence of Protic Non-Solvents on Nucleation in Thin Film Solutions

In order to investigate whether formation and dissolution of the ordered structures in thin film solutions can be controlled by simply changing the vapor pressure of a protic non-solvent, more complex off-equilibrium experiments were designed. Experiments were performed under dry air conditions and in a vapor

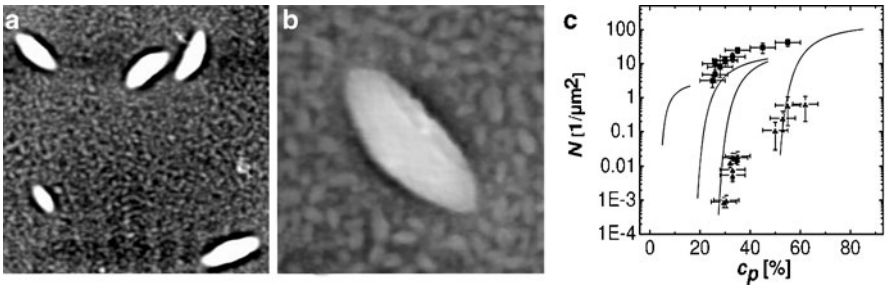

Fig. 9 (**a, b**) AFM topography images presenting a bimodal distribution of ordered ellipsoidal structures of a 40 ± 3 nm thick film spin-coated from chloroform solution. The film had been exposed using off-equilibrium experiments to a mixture of chloroform and methanol vapor under dry air conditions (obtained by flushing the sample chamber, before film swelling, with a N_2 flow) at $c_p = 30\%$ (for 30 min) and at higher $c_p = 45\%$ (for 2 min). (**c**) Representation of nucleation density N against polymer concentration c_p as determined from off-equilibrium experiments carried out by exposing thin films to chloroform vapor under dry air conditions and adding methanol (*filled spades*) or toluene (*filled clubs*). Off-equilibrium experiments carried out by exposing thin films to THF vapor under ambient air conditions are indicated by *filled squares*. Note that dry air conditions have been obtained either by using P_2O_5 (in the case of toluene) or by flushing the sample chamber with N_2 flow (in the case of methanol) before the film swelling process. The *lines* are the fits for data points obtained under (from *right* to *left*): dry, less humid, more humid and highly humid air conditions (see Fig. 13a). Sizes of images are (**a**) 10×10, and (**b**) $3 \times 3\,\mu m^2$

atmosphere with the controlled addition and subsequent removal of water or methanol molecules. Conditions were realized by flushing the sample chamber with N_2 flow before performing the swelling of the film. During formation and dissolution of ordered structures, c_P was kept relatively constant (small fluctuations around this value could not be excluded). The two sets of experiments – either using water or methanol molecules in the surrounding gas phase – yielded similar results. Therefore, only results for the addition and removal of methanol are presented here.

First, a 40 ± 3 nm thick solid film of PS_{63}–$(PBLGlu_{37})_8$ heated to a temperature of 35°C was exposed for 10 min to chloroform vapor inside a sample chamber, which was kept approximately at room temperature. The swelling of this film started under dry air conditions. Then, the temperature of the film was lowered until the film was swollen to $5 \pm 2\%$ of polymer.

After 2 min at $c_P = 5 \pm 2\%$, the sample temperature was raised, causing an increase of c_P to $34 \pm 5\%$. The sample was kept at this concentration for about 10 min. The morphology resulting at this stage is shown in Fig. 10a. No isolated objects were observed within the resolution of OM.

After these 10 min, methanol vapor was added in the sample chamber by opening a valve to a supplementary chamber where methanol had been heated to 55°C. After about 5 min, one could observe the appearance of isolated objects. These objects became better developed and more clearly visible after about 9 min (see Fig. 10b).

Then, methanol molecules were removed from the sample chamber (the valve between the two chambers had been closed and the chamber purged with a very weak N_2 flow for 15 min). After 5 min, the isolated objects started to dissolve and almost

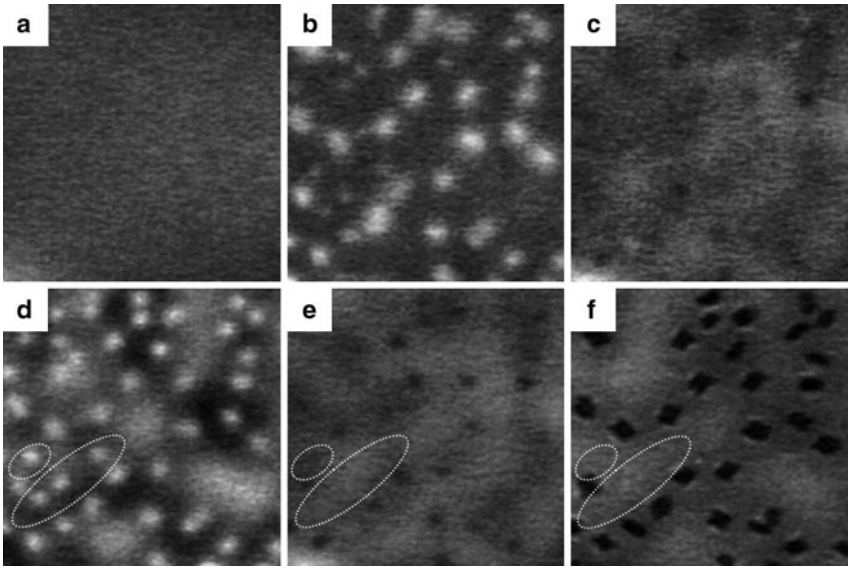

Fig. 10 Structure formation and dissolution in a 40 ± 3 nm thick film of PS_{63}–$(PBLGlu_{37})_8$ swollen in chloroform vapor at about $34 \pm 5\%$ of polymer: (**a**, **c**, **e**) no methanol molecules present; (**b**, **d**) small amounts of methanol molecules present; (**f**) totally dried film. Before performing the swelling of the thin solid film, the sample chamber was flushed with N_2 flow in order to create dry air conditions. Regions marked with *dotted lines* show (**d**) presence, (**e**) disappearance, and (**f**) reappearance of structures. Size of all OM images is 50×50 µm^2

all of them had disappeared after 19 min (see Fig. 10c). Two minutes later, methanol molecules were added again by opening the valve between the two chambers. Isolated objects reappeared after about 2 min and developed into better defined objects during the following 10 min (see Fig. 10d). This procedure of adding and removing methanol was repeated a second time. As expected, the isolated objects dissolved within about 15 min (see Fig. 10e). However, this time, not all objects were dissolved completely. Thus, when adding methanol molecules again, after about 5 min, the previously dissolved objects appeared again, as shown in Fig. 10f (after complete drying of the film). However, not all of the previously visible structures reappeared. Some of them (formed after the second addition of methanol molecules) dissolved completely when methanol molecules were removed and did not reappear again when methanol molecules were added for the third time (compare the regions inside the dotted elliptical forms in Fig. 10d–f).

Detailed features of these isolated objects being formed in film solutions were studied by AFM after completely drying the film solutions. In Fig. 11, two AFM topography images are shown for objects similar to those visible in Fig. 10f. As can be seen, two types of populations of ordered structures were present: ellipsoidal structures, which were most probably formed by nucleation from a single seed, and "double" ellipsoidal structures, which may have been formed from two neighboring seeds. Seeds may have resulted from ordered structures that were only partially

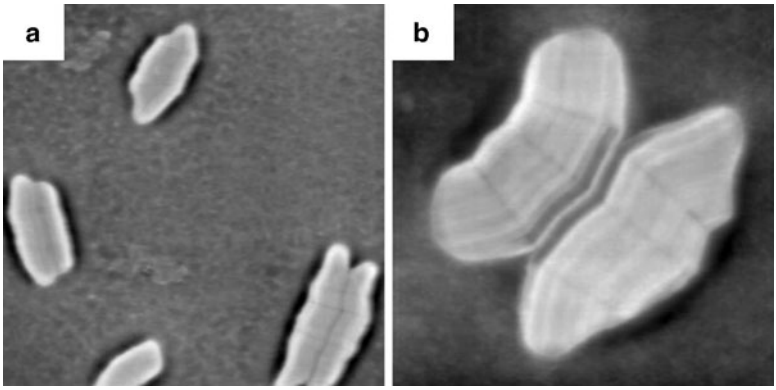

Fig. 11 AFM topography images showing ordered structures obtained in a 40 ± 3 nm thick film of PS_{63}-$(PBLGlu_{37})_8$ swollen in chloroform vapor, under dry air conditions (the sample chamber was flushed with N_2 flow before film swelling) and at about 34% of polymer. Note that the two images are from the same film but of slightly different regions on the film surface. Sizes of images are (**a**) 10×10, and (**b**) $4 \times 4\,\mu m^2$

dissolved. From such seeds, a "double" structure (see Fig. 11b) has probably grown when re-adding non-solvent molecules. No such seeds were found when the ordered structures were totally dissolved.

In summary, adding small amounts of water or methanol molecules to the surrounding gas phase can induce nucleation and growth of ellipsoidal ordered structures up to more than 10 µm in size. Without such additions, nucleation does not occur at such low polymer concentration. It can be concluded that water or methanol molecules complexed the PBLGlu and, consequently, increased the interfacial tension between the ordered structures and solution, which, in turn, facilitated structure formation by decreasing the polymer solubility. After removal of water or methanol molecules, at constant c_P, these ordered structures dissolved due to the increased polymer solubility.

Ordered structures reappeared at the same c_P when water or methanol molecules were added again to the surrounding gas phase. This structure formation/dissolution cycle can be repeated, which proves the reversibility of the process of structure formation and dissolution.

Finally, all these results support the validity of the concept of complexation of PBLGlu by protic non-solvent molecules via hydrogen-bonding interactions. Such complexes exhibit a lower solubility $c_{critical}$, which explains the dependence of the interfacial tension σ on the degree of humidity of the surrounding gas phase. Among the various possibilities for hydrogen bonding, the two hydrogen bonds of type C=O···H–O between the oxygen atom of the ester carbonyl group and hydrogen atom of water seem to be most favorable (see Fig. 12). The ester group is located at the exterior of the PBLGlu helix and is not otherwise involved in hydrogen bonding. As already indicated, the secondary amide groups of the PBLGlu backbone, on the other hand, are involved in intramolecular hydrogen bonding, stabilizing the α-helical conformation of PBLGlu, and are hidden inside the core of the helix.

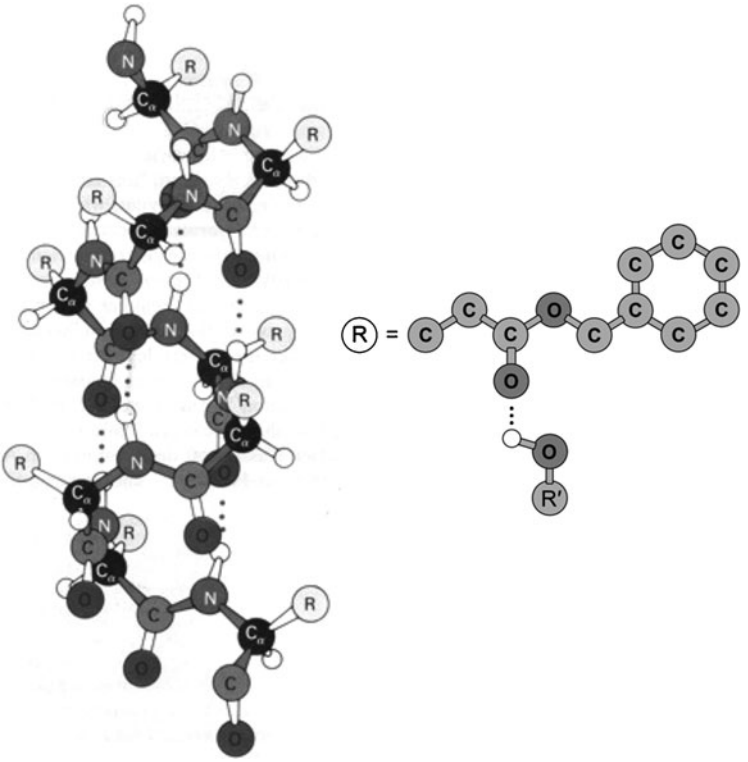

Fig. 12 Representation of a PBLGlu α-helix (taken from [1]) and the coordination of water (or alcohol) molecules to the ester carbonyl group in the side chain via hydrogen bonding

3.5 Origin of Bimodal and Multimodal Distributions in Size of the Resulting Ordered Objects

So far, mainly OM has been used to directly observe in real time the nucleation and growth of ordered polypeptide solid ellipsoidal structures in thin solution films. Detailed characterization of these ellipsoidal structures will be given in this section. In particular, more information will be presented on how these structures form at the molecular level, and about the forces that lead to formation of ellipsoidal ordered structures with an aspect ratio of about 2. It will also be explained how two different populations of ordered structures can be generated in a single film.

The chosen experimental approach could not prevent slight fluctuation of c_P around its set value by about 2–3%, including small drifts of c_P. Experimentally, it is often observed (after exposure of the films to solvent vapor and subsequent complete drying) that in a single sample, several types of structures are generated, differing basically only in size. In order to address this behavior, the consequence of an abrupt change in c_P, say, from c_P to $c_P + 15\%$, was examined. Figure 13 shows a

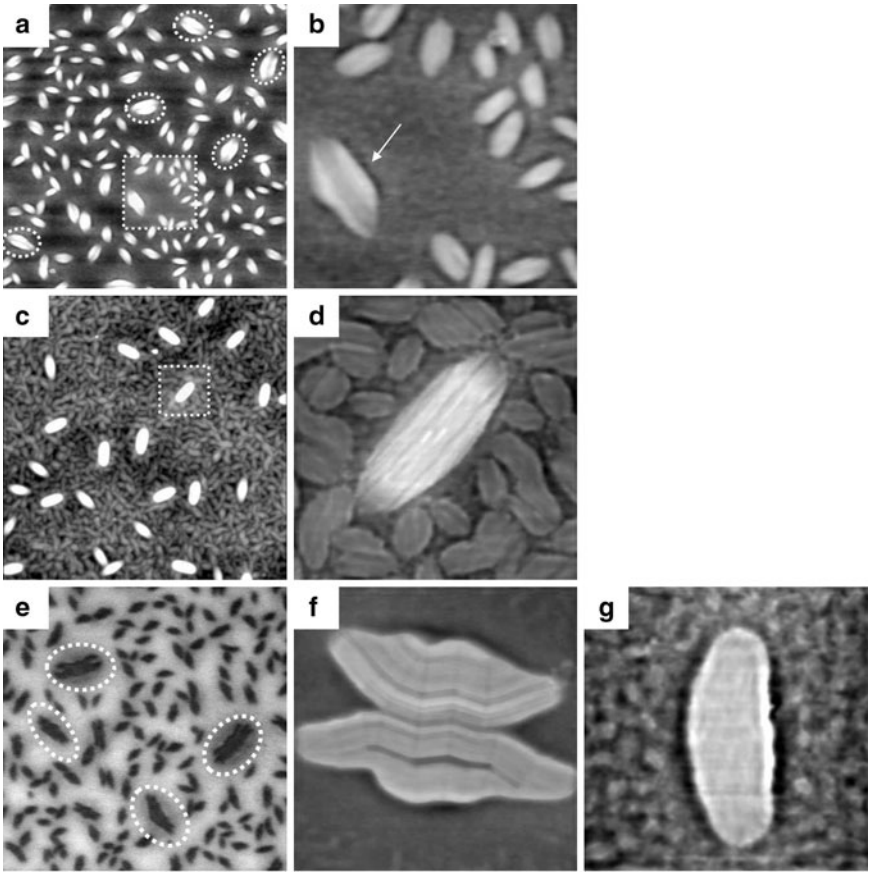

Fig. 13 (**a–d**, **f**, **g**) Series of AFM topography images and (**e**) an OM micrograph showing different distributions of ordered structures on the film surface. (**a**, **b**) Bimodal distribution of a 50 ± 3 nm thick film prepared under dry air conditions (off-equilibrium experiment) at $c_{p1} = 53\%$ (for 10 min) and at slightly higher $c_{p2} = 56\%$ (for 15 min), respectively. (**c**, **d**) Bimodal distribution of a 25 ± 2 nm thick film prepared under ambient air conditions (off-equilibrium experiment) at $c_{p1} = 30\%$ (for 15.5 h) and at higher $c_{p2} = 45\%$ (for 7 h), respectively. (**e–g**) Multimodal distribution of a 40 ± 3 nm thick film prepared under ambient air conditions (off-equilibrium experiment) at $c_{p1} = 18\%$ (for 2 h), at higher $c_{p2} = 25\%$ (for 30 min), and at $c_{p3} = 45\%$ (for 5 min), respectively. The *dotted squares* indicate a zoomed-in region. *Arrow* in (**b**) and *dotted* regions in (**a, e**) indicate large objects. The sizes of images are (**a**) 10×10, (**b**) 2.5×2.5, (**c**) 9.5×9.5, (**d**) 1.25×1.25, (**e**) 45×45, (**f**) 4.5×4.5, and (**g**) $2.25 \times 2.25\,\mu m^2$

series of AFM topography images and an OM micrograph of different distributions of ordered structures observed in films after various experimental conditions.

In a first experiment, a 50 ± 3 nm thick film was exposed to chloroform vapor under dry air conditions (off-equilibrium experiment) at two different concentrations: $c_{p1} \approx 53\%$ and subsequently at a slightly higher concentration, $c_{p2} \approx 56\%$. The experiment was followed in real time under the optical microscope. A spin-coated film

was initially swollen to 5% of polymer and was then concentrated to c_{p1}. After about 10 min, the concentration was again increased (to c_{p2} of ca. 56%) by increasing the film temperature by 0.5°C. After about 15 min at c_{p2}, the sample was completely dried and investigated by AFM.

The two AFM topography images of Fig 13a, b show the resulting distribution in size of the obtained ordered structures. As can be seen, the ordered structures were of ellipsoidal shape, randomly but evenly distributed over the whole film surface. What is interesting in these images is the fact that there were two distinct distributions of ellipsoidal structures, which could be differentiated according to their size. There were relatively few structures that averaged about 1 µm along their longer axis (referring to the structures inside the dotted ellipses in Fig. 13a and to the structure indicated by the black arrow in Fig. 13b). These larger structures were formed at the lower c_{p1} and could be directly detected by OM. However, the majority of objects were smaller and only slightly exceeded an average size of 500 nm. It may be assumed that the two types of structures appeared at c_{p1} and $c_{p2,}$ respectively.

In a second off-equilibrium experiment (see Fig. 13c, d), this time performed under ambient (humid) air conditions, the ordering process was followed in a 25 ± 2 nm thick film exposed for a long duration (tens of hours) to chloroform vapor. After swelling of the film (up to 5% of polymer), c_p was increased to $c_{p1} = 30\%$ and the sample was kept for 15.5 h. After reaching the concentration c_{p1}, ellipsoidal 3D structures formed rapidly, typically within a few minutes, as confirmed directly by OM (not shown) and later on by AFM (see the white ellipsoidal structures in Fig. 13c). No further changes were detectable for the rest of time (ca. 15 h) at c_{p1} and structures did not grow further.

Finally, the c_{p1} in the film was increased quickly to $c_{p2} = 45\%$ for 7 h before rapidly drying the sample. Subsequent AFM analysis (Figs. 13c, d) showed that the larger ellipsoidal objects detectable by OM were surrounded by smaller structures of similar shape (for each population, both shape and size were rather uniform). These smaller structures were formed at the concentration c_{p2} and contained almost all available material. The ordered structures were separated by narrow depressions containing only very few molecules (depleted regions).

The above and additional experiments (not shown, under both dry and ambient air conditions), proved that the size of the observed objects did not increase measurably beyond the size reached after a few minutes of exposure at c_P, even when the time was increased to more then 10 h. Why did growth not continue?

First, it has to be emphasized that rather low values of c_p, very close to the $c_{critical}$, were chosen. Under such conditions only few nuclei were formed, which facilitated their observation by OM. As already discussed, once a nucleus has formed, it continues to grow, taking up molecules from the surrounding until c_P of the remaining solution dropped below the $c_{critical}$ (refer to Fig. 13c, d). At this moment, the reservoir of molecules available for insertion into the ordered structures became exhausted and growth stopped.

Accordingly, the bimodal distribution in size observed in Fig. 13c, d can be explained in the following way: The bigger structures were nucleated and grew at

the lower c_{p1}. The comparatively lower number density of objects was determined by the value of c_{p1} (see Fig. 8a). As these objects grew, they finally exhausted the reservoir of available molecules and thus growth came to a halt. However, when the polymer concentration was subsequently increased to a significantly higher value $c_{p2} > c_{critical}$, a second process of nucleation and growth of structures was initiated. Because the initial distance to $c_{critical}$ was quite large, the resulting number of nuclei was higher because there was a higher probability for nucleation (see e.g. Fig. 8a). This second nucleation and growth process was again stopped, either when the reservoir of available molecules became exhausted (see Fig. 13a, b) or when the growing structures coalesced (see Fig. 13c, d).

Based on this explanation, any multimodal distribution in size can be obtained just by increasing the c_P in an appropriate number of steps. Figure 13e, g present an additional off-equilibrium experiment that was also performed under ambient air (i.e., humid) conditions. The ordering process in a 40 ± 3 nm thick film was again followed in real time during exposure to chloroform vapor at three subsequent values of c_P: $c_{p1} = 18\%$ (for 2 h), a slightly higher value of $c_{p2} = 25\%$ (for 30 min), and $c_{p3} = 45\%$ (for 5 min). Note that c_{p1} was chosen close to the solubility limit, and small concentration fluctuations (caused by temperature fluctuations of ca. 0.1°C) may have crossed $c_{critical}$ temporarily. Thus, growth may have been interrupted by short periods of partial dissolution.

OM had confirmed (see Fig. 13e) that two populations of structures were formed at c_{p1} and c_{p2}. AFM allowed the identification of a third population of structures that formed at c_{p3} (see the multitude of small structures, less then 100 nm^2, in Fig. 13g). In Fig. 13g, one can see an ellipsoidal structure formed at c_{p2} that is surrounded by the much smaller objects formed at c_{p3}.

Figure. 13f presents a structure of about 5 µm formed at c_{p1}. This type of structure is marked by the dotted ellipses in the OM of Fig. 13e. The shape of this structure indicates a "tandem-like" structure, which is most probably the result of the small fluctuations of c_{p1} in between $c_{p1\,max}$ and $c_{p1\,min}$. The nucleus formed initially at $c_{p1\,max}$ and started to grow, but was then partially dissolved when c_{p1} became $c_{p1\,min} < c_{critical}$, assuming that some seeds could remain. If two such seeds remained close together, a tandem-like structure could grow when the polymer concentration increased again to $c_{p1} > c_{critical}$. Such a multipart structure may thus be the result of nucleation by self-seeding.

3.6 Kinetics of Growing Ordered Objects

It should be pointed out that in all experiments, the resulting structures were detectable by OM after a few minutes. Certainly, under an optical microscope, such structures can only be detected when their size becomes large enough (≈500 nm). So, how fast did these structures grow? In a control experiment, c_P was increased rapidly (within a few seconds) from 5 to 100%. Only small and less well-defined objects of about 100 nm were formed (see Fig. 14). No large ordered structures

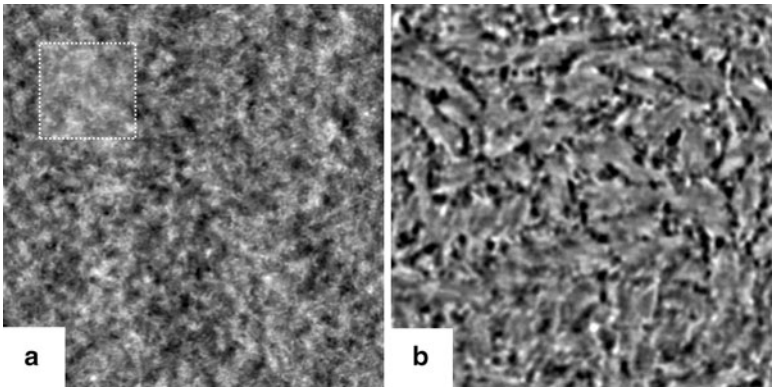

Fig. 14 TM-AFM typical images (**a** topography, **b** phase) showing the surface of a 30 ± 2 nm thick PS_{63}–$(PBLGlu_{37})_8$ film after its exposure to chloroform vapor for 5 min and rapid drying. This film was first swollen at about 5% of polymer (the film temperature was decreased from 35 to $-5°C$). After swelling, the film was then heated very fast (in about 10 s the film temperature was increased from -5 to 65°C) in order to extract all the solvent from the film. No large ordered structures could be observed. The *dotted square* in (**a**) indicates the region that is shown magnified in (**b**). The sizes of images are (**a**) $2 \times 2\,\mu m^2$, and (**b**) $500 \times 500\,nm^2$

were observed (see Fig. 14a). Consequently, the molecules need more than a few seconds to order themselves on large scales. For example, during spin-casting the solvent evaporates very quickly and, consequently, the molecules are deposited on the substrate in a non-organized fashion. Thus, the time of several seconds during which solvent evaporates is not sufficient for ordering. Similarly, when the c_p was increased rapidly from 5 to 100%, molecules did not have time for ordering at large scales (larger than about 100 nm, see Fig. 14b). During such rapid drying, the molecules pass any polymer concentration c_P (for example 30%) in much less than a second, which is not enough to allow a distinct nucleation and growth process yielding well-defined ordered objects. On the other hand, the above experiments proved that molecules could become ordered into larger ellipsoidal structures within about 2 min when exposed to solvent vapor under constant conditions. Thus, it may be concluded that molecules needed more than a second but less then 2 min to form micrometer-sized ordered structures in solution.

3.7 Origin of the Anisotropic Shape of the Resulting Ordered Objects

As previously shown (Figs. 3 and 5), it was also attempted to follow the kinetics of structure formation. In Fig. 3, at c_p of about 53%, the first indication of the formation of ordered structures became visible after about 25 min. At this concentration, the growth process was sufficiently slow to be followed in real time. In addition,

the nucleation density was low enough so that individual objects were sufficiently separated and could be resolved by OM. These structures, as revealed by AFM analysis after total drying of the film, possessed an anisotropic shape (ellipsoidal, with an aspect ratio of length to width of about 2). A similar anisotropic shape has been observed for all experiments performed with the polymer system of this study. So, why do the observed structures grow laterally faster in one direction and slower along the orthogonal direction?

To answer this question, anisotropic growth has to be related to the intermolecular interactions between the molecules. One has to find out which is the most favorable way for molecules to arrange with respect to these two growth directions. It is known that PBLGlu α-helices possess high dipole moments (about 3.5 Debye per unit and sites for hydrogen-bonding interactions. Thus, the mechanism of structure formation will most probably be based on strong dipole–dipole interactions between rather rigid PBLGlu α-helices. Note that, at larger scales the grown objects have to be electrically neutral, implying that the high dipole–dipole moments have to be compensated for. Directional hydrogen-bonding interactions may contribute to lateral ordering of PBLGlu α-helices (normal to the long axis of the α-helix).

Two possibilities could be causing an asymmetric growth of ellipsoidal structures: (1) anisotropic transport phenomena and/or (2) directional intermolecular interactions. The observed 3D structures were formed in solution, in which molecules can move easily. The large lateral size of the formed objects (much larger than the molecular length-scale) and their random orientation in space (the long axis of the ellipsoidal objects does not exhibit any preferred directions) indicate that anisotropic transport within the solution is probably not responsible for the shape. Therefore, anisotropy in lateral growth may be attributed to specific intermolecular interactions between the α-helices. These interactions will affect the growth rate in various directions.

Figure 15 shows a rather complex morphology, which will help to identify a potential growth mechanism of ordered structures. This morphology resulted from exposure of a 100 ± 5 nm thick film to chloroform vapor under dry air conditions (off-equilibrium experiment) at $c_p = 54 \pm 5\%$ for 25 min. Probably due to the high amount of available molecules in such a thick film and the correspondingly high nucleation density, the shape of the formed structures is not unique, varying from isolated ellipsoidal to "meandering" structures (see Fig. 15a, b).

As an attempt to explain these meandering structures, one may assume that they resulted from coalescence of many initially ellipsoidal structures that coalesced during growth. The initial ellipsoidal structures are indicated in Fig. 15c. These initial structures grew in the plane of the substrate in the fast (f) and the slow (s) direction. After coalescence, growth stopped in one direction.

The clearly visible lines (represented by broken white lines in Fig. 15c, d) are thus supposed to be the result of such coalescence between initial structures during the growth process. The dotted black lines in Fig. 15d indicate the variable directions of the long axis of the initially nucleated structures. The long axis also represents the orientation of parallel stripes building up these objects. These stripes could be

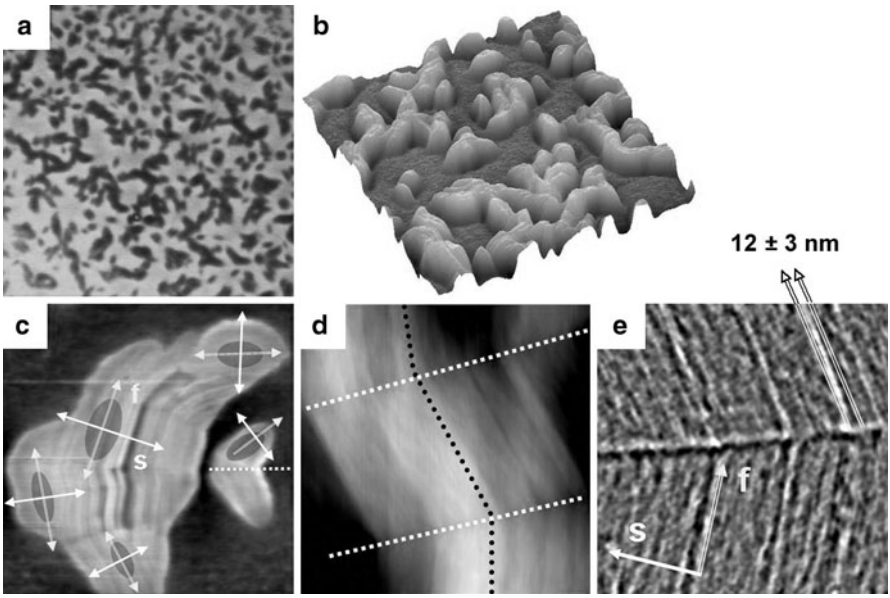

Fig. 15 Series of OM (**a**) and AFM (**b**, **c**, **d** topography, **e** phase) images showing the coalescence of ordered structures in a 100 ± 5 nm thick film prepared under dry air conditions (off-equilibrium experiment) at $c_p = 54 \pm 5\%$ for 25 min. The *arrows* marked *f* indicate the fast-growing direction (along the normal to chain axis of α-helices). The *arrows* marked *s* indicate the slow-growing direction (parallel to chain axis of α-helices, i.e. normal to main chain axis). The *white dotted lines* represent a coalescence line, and the *black dotted lines* indicate the random orientation of initially nucleated structures. The *elliptical forms* in (**c**) are the initial ellipsoidal structures. The sizes of images are (**a**) 100×100, (**b**) 19×19, (**c**) 5×5, (**d**) 1.25×1.25, and (**e**) $0.75 \times 0.75\,\mu m^2$

clearly distinguished by examining the surface of the assembled structures by AFM. Their average width (see Fig. 15e), was measured to be 12 ± 3 nm. This size is comparable to the molecular dimension of the investigated molecule, more precisely, to the length of two α-helices in series (see Fig. 1c).

Such long, straight, parallel stripes have been always observed on top of the ellipsoidal structures (see the inset in Fig. 3f). A typical example is also shown at a higher resolution in Fig. 16a. From the height profile presented in Fig. 16b, the average width of the stripes is about 12 ± 3 nm. Taking into account the above considerations, one may conclude that comparatively strong lateral interactions between α-helices (hydrogen-bonding interactions) favor fast growth along the axis normal to α-helical chain, i.e., along the long axis of the ellipsoidal structures. Slow growth then results in the direction along the chain axis of α-helices and will determine the width of the ellipsoidal structures. These observations, together with the average width of the stripes of about 12 ± 3 nm, suggests a model for a possible molecular organization inside the stripes (in the plane direction of the ellipsoidal ordered structures; see Fig. 16c).

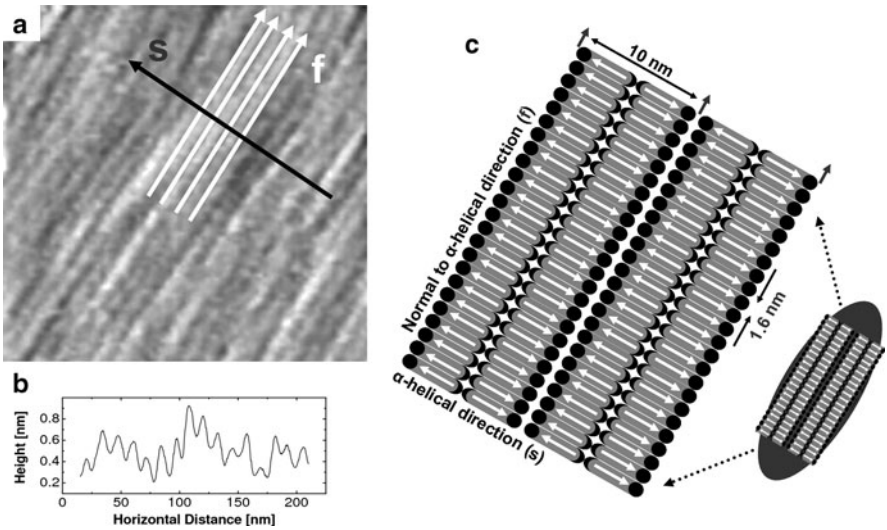

Fig. 16 (**a**) AFM topography image showing the parallel straight stripes on top of an ellipsoidal structure. (**b**) Height profile made in the region indicated by the *arrow* marked *s* in (**a**). The average distance between the stripes was about 12 ± 3 nm. (**c**) Representation of a possible arrangement of α-helices inside the parallel stripes observed on top of ellipsoidal structures and indicated in (**a**) by *arrows* marked *f*. The *white arrows* indicate the dipole moments. The size of image (**a**) is: $250 \times 250\,\text{nm}^2$

3.8 Growth in the Out-of-Plane Direction of the Resulting Ordered Objects

The out-of plane growth is based on interdigitation of α-helices (interdigitation takes place along vertical direction; see later). An interdigitated molecular arrangement can compensate for the high dipole–dipole interaction between α-helices during the course of growth.

Each α-helix carries a considerable permanent dipole moment of about 3.5 Debye per unit. Its value can be approximated by placing 0.5–0.7 positive unit charge near the N-terminus and 0.5–0.7 negative unit charge near the C-terminus of the α-helix. An interdigitated molecular arrangement with alternating directions of the peptide blocks from neighbouring molecules (see Fig. 16c) allows the compensation of these high dipole moments of α-helices. Such an arrangement can also explain, along and normal to the PS chain axis (as indicated in Fig. 1), a 2D growth of structures. It should be noted that PBLGlu α-helices have the tendency to be aligned parallel to the substrate due to the high dipole interactions between PBLGlu α-helices and the hydrophilic substrate. It seems even possible to link PBLGlu α-helices via hydrogen bonds to OH groups of the UV/ozone-treated silicon substrate.

Figure 17 presents a case where clear steps in height inside ordered structures could be observed. A thinner region inside an ordered object (see the dark part in

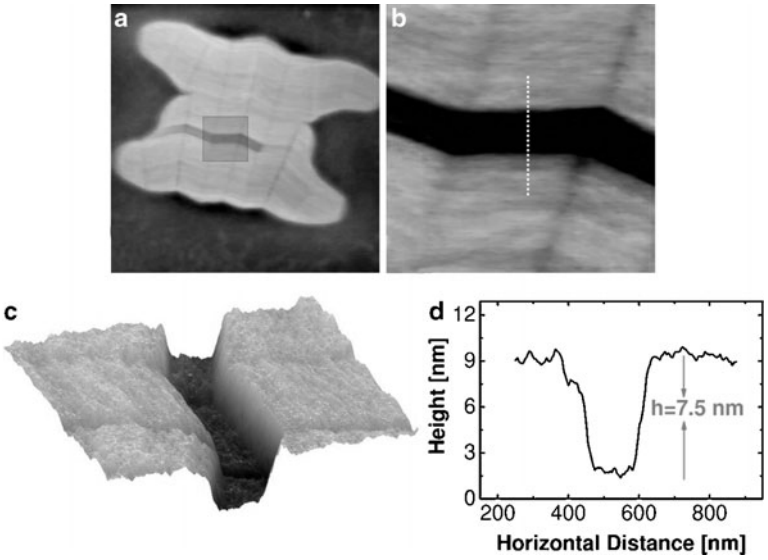

Fig. 17 (**a**) AFM topography image showing a complex coalesced multistructure. (**b**) Magnification of *grey square* in (**a**) showing a defect. (**c**) 3D representation of the defect shown in (**b**). (**d**) Height profile made in the region indicated by the *white broken line* in (**b**). The sizes of images are (**a**) 5×5, (**b**, **c**) $1 \times 1\,\mu m^2$

Fig. 17b, c) offered a possibility to visualize how the ordered structures are built up in the direction normal to the surface plane. A cross-section (see height profile in Fig. 17d) yielded a depth of this zone of about 7.5 nm. This value is comparable to the estimated total length of the molecule along the PS chain axis of 7.5 nm (see Fig. 1c). Such steps within the ordered structures, having a mean height about 7.5 nm were observed quite frequently in experiments. Thus, one may assume that the PS_{63}–$(PBLGlu_{37})_8$ molecules are stacked with the PS main chain axis normal to the substrate plane.

On the basis of the experiments shown above, one may suppose that the growth in height of the observed ordered structures can be explained by a stratified arrangement, i.e., lamellar layering (see Fig. 18). Such an arrangement of the peptide blocks would avoid the unfavorable contact between the PS segments and the hydrophilic silicon substrate.

3.9 Concerted Changes of the Growth Direction: Dependence on Polymer Architecture

Finally, there is an interesting and so-far unexplained feature that appeared when structures became larger than about 1 µm. In Figs. 11, 13f, 15c–e and 17a–c, one can detect concerted changes in the growth direction for these large-scale structures.

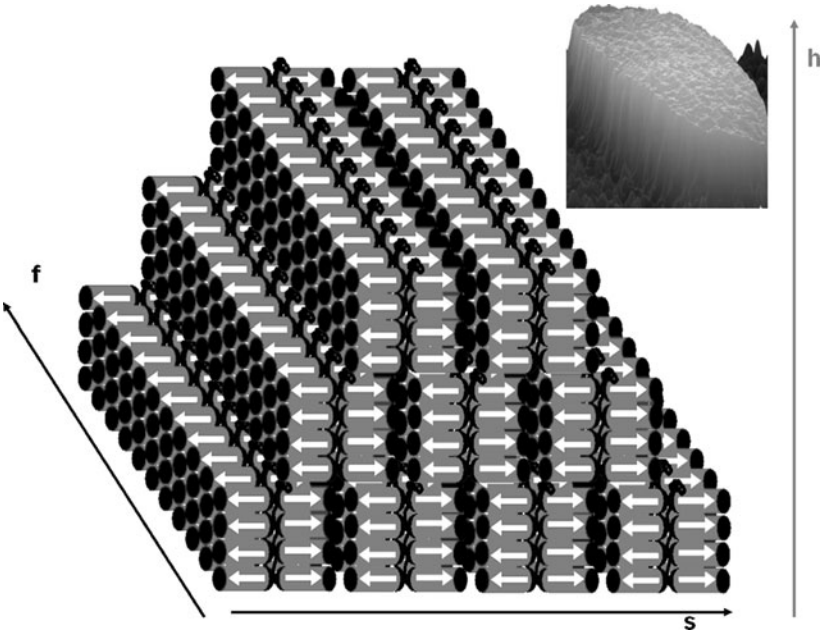

Fig. 18 Possible 3D molecular organization model of PS_{63}–$(PBLGlu_{37})_8$ heteroarm star block copolymer. The *inset* represents a 3D AFM topography image showing a typical ellipsoidal solid structure

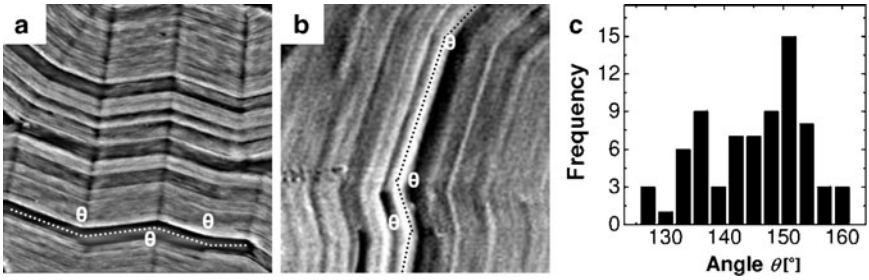

Fig. 19 (**a**) TM-AFM phase image showing a magnification of the film surface presented in Fig. 13f. (**b**) TM-AFM phase image showing a magnification of the film surface presented in Fig. 15c. (**c**) Distribution of orientation angle (θ) showing the number of appearances of a certain orientation angle over 100 measured values. The *white* and *black dotted lines* in (**a**) and (**b**) emphasize the orientation angles denoted by θ. Sizes of images are (**a**) 1×1 , and (**b**) $1.74 \times 1.74\,\mu m^2$

A multitude of long, parallel straight lines show a simultaneous change in orientation, causing a change of the orientation angles by a well-defined value. Examination of a large number of such large-scale structures yielded an angle (denoted by θ) of about 135–157° between two consecutive domains (see Fig. 19).

The most frequent values were centered around 136° and 151°, with the occurrence of 151° being almost twice as often as that of 136°. It may be concluded

that the large scale structures formed at a c_P close to $c_{critical}$ did not grow in a straight line to big sizes, but that concerted and cooperative discrete changes in orientation angle occurred at distances of the order of 1 µm.

One may ask if this effect of changing orientation depends on macromolecular polypeptide architecture. To answer this question, various other polypeptide systems having different architecture were examined. Thin films made of PBLGlu homopolymer, linear PS_{52}–$PBLGlu_{104}$ diblock copolymer, linear PS_{52}–$PBLGlu_{31}$ and star shaped PS_{63}–$(PBLGlu_{37})_8$ were exposed simultaneously to chloroform vapor under ambient air conditions in an "open" system with a continuous but slow evaporation of gas (estimated to be about 0.2 mL/h) from the sample container to the environment. This allowed a slow increase in the polymer concentration c_P.

Under such conditions, the initial polymer concentration c_P in the films was estimated to be about $50 \pm 20\%$. After 195 h, the films were taken out of this sample chamber and dried completely at room temperature. Investigating all four samples by OM and AFM demonstrated a clear ordering process (see Fig. 20). OM

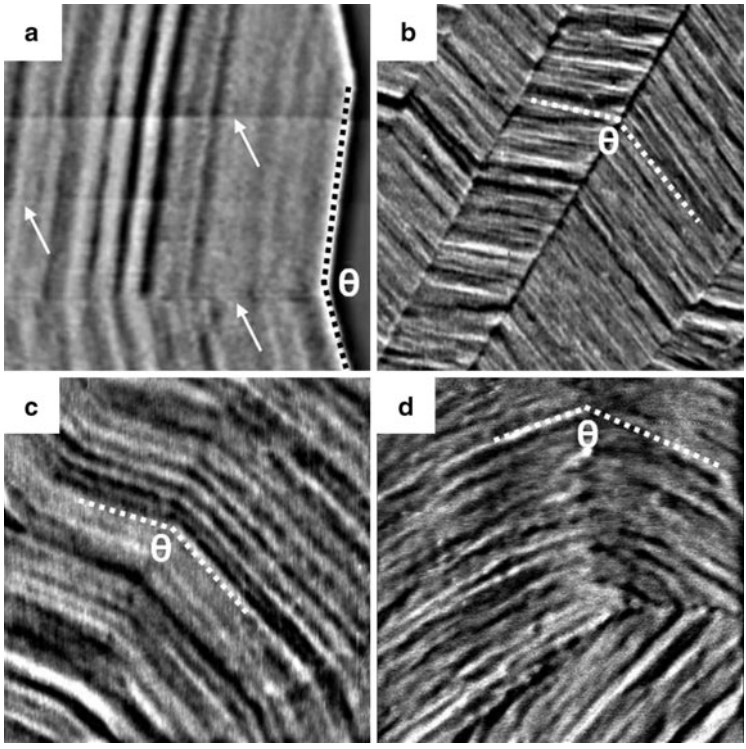

Fig. 20 TM-AFM phase images showing the morphology of (**a**) a 54 ± 2 nm thick film made of PS_{63}–$(PBLGlu_{37})_8$ star block copolymer; (**b**) a 60 ± 3 nm thick film made of PS_{52}–$PBLGlu_{31}$ diblock copolymer; (**c**) a 65 ± 3 nm thick film made of PS_{52}–$PBLGlu_{104}$ diblock copolymer; and (**d**) a 70 ± 3 nm thick film made of PBLGlu homopolymer. All three films were exposed to chloroform vapor for 195 h under ambient air conditions in an "open" system. The *white arrows* in (**a**) indicate artifacts (*horizontal lines*) resulting from removal of some noisy lines acquired during TM-AFM scanning. Sizes of images are (**a**) 1.75×1.75, (**b**, **c**) 1.5×1.5, and (**d**) $0.5 \times 0.5\,\mu m^2$

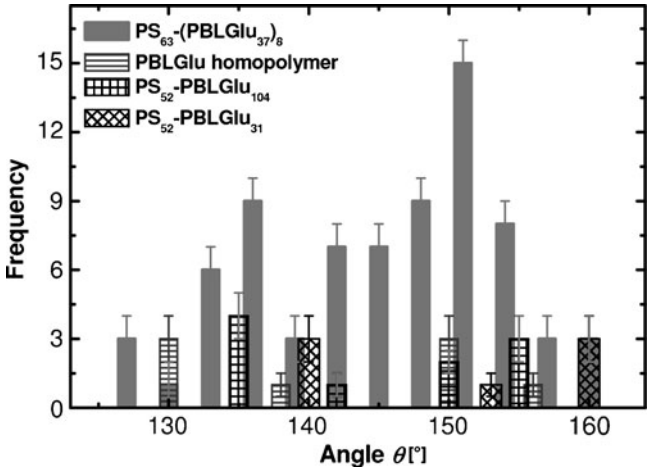

Fig. 21 Orientation angle (θ) distribution showing the number of appearances of a certain orientation angle over 100 measured values for: PS_{63}–$(PBLGlu_{37})_8$, PBLGlu homopolymer, PS_{52}–$PBLGlu_{104}$, and PS_{52}–$PBLGlu_{31}$

(not shown) confirmed that large-scale ordered structures, up to tens of micrometers, were obtained for all systems. As revealed by AFM, all four polymer systems showed micrometer-long, straight parallel stripes that often changed their orientation (see Fig. 20). The measured orientation angles for all four polymer systems were found to be in the range of 130–160°. A summary of an extended study is presented in Fig. 21, which clearly demonstrates that the concerted discrete changes in orientation occurred in a similar way in all the studied polypeptide systems, independent of architecture.

4 Conclusions

OM allows the direct observation in real time of nucleation and growth in thin solution films, here demonstrated for the formation of ordered polypeptide structures. The variation of the nucleation density (number of nuclei per area) with concentration could be determined by combining OM and AFM. Interestingly, the nucleation density was sensitively affected by the humidity of the surrounding gas phase. For example, in dry air up to about 50% of polymer could be homogeneously dissolved in chloroform, whereas only about 20–30% of polymer could be dissolved under ambient air conditions without formation of ordered structures. The influence of humidity can be expressed in terms of the c_{critical}, below which no structures were formed. Increasing the humidity of the surrounding gas phase led to a decrease of the value of the c_{critical}. The functional dependence of the number of ordered objects per unit area on c_{p}, in combination with theoretical considerations, allowed the determination of a value for the interfacial tension σ between the polymer and the solution. Accordingly, the decrease in c_{critical} with humidity can be linked to

an increase in σ. It is proposed that complexation between water molecules and PBLGlu chains, favored by hydrogen-bonding interactions, is responsible for the decrease of the "solubility" of the polymer in chloroform, leading to ordering at even very low c_p. Furthermore, it could be demonstrated that other protic solvents can also cause a similar decrease in solubility. Consequently, the solubility of complex molecules like polypeptides (which contain sites of different polarity, hydrophilicity, or hydrophobicity) not only depends on the quality of the solvent chosen but can also be varied by the presence of small amounts of a non-solvent, which nonetheless can interact locally with specific sites on the molecule.

At a given concentration, the resulting ellipsoidal structures grew to a certain size and then growth stopped. However, after an abrupt increase of the concentration, additional structures of smaller size but of similar shape formed. This arrest of growth was due to a decrease of the concentration of the surrounding solution below supersaturation, i.e., the reservoir was depleted by molecules integrated into the ordered structures. Consequently, such two-step growth processes led to a bimodal distribution in size of ordered structures in the film.

All structures possessed an anisotropic ellipsoidal shape, which can be attributed to asymmetric growth in lateral directions. The surface of these structures exhibited straight parallel stripes of a width similar to the molecular dimension of the peptide blocks. On the basis of these results, it can be concluded that anisotropic structure formation is due to specific directional interactions acting along the various axes of the molecules. Intermolecular hydrogen bonds act normal to long axis of PBLGlu α-helices. This might explain the existence of parallel straight stripes over large scales and spaced at a molecular distance. The existence of steps in height of molecular dimension, along the axis normal to substrate, suggests a stratified arrangement, i.e., lamellar layering of the molecules.

Large-scale structures formed at a polymer concentration slightly above $c_{critical}$ showed growth morphologies dominated by concerted discrete changes in orientation of a multitude of parallel stripes. The experiments performed in this work proved that the ellipsoidal morphology and the appearance of concerted changes in orientation during the growth of large-scale structures depended on neither the environmental conditions nor the polymer architecture. Thus, the ordering process of polypeptide-based copolymers and the resulting morphology were basically controlled by the solubility of the polymer.

Acknowledgements We are indebted and grateful to Hildegard Kukula for polymer synthesis. We acknowledge financial support provided through the European Community's "Marie-Curie Actions" under contract MRTNCT- 2003-505027 [POLYAMPHI]. Use of the Center for Nanoscale Materials was supported by the US Department of Energy, Office of Science, Office of Basic Energy Sciences, under Contract No. DE-AC02-06CH11357.

References

1. Stryer L (1988) Biochemistry. W H Freeman, New York
2. Börner HG, Schlaad H (2007) Bioinspired functional block copolymers. Soft Matter 3: 394–708

3. Lee M, Cho B-K, Zin W-C (2001) Supramolecular structures from rod-coil block copolymers. Chem Rev 101:3869–3892
4. Klok H-A, Lecommandoux S (2006) Solid-state structure, organization and properties of peptide–synthetic hybrid block copolymers. Adv Polym Sci 202:75–111
5. Muthukumar M, Ober CK, Thomas EL (1997) Competing interactions and levels of ordering in self-organizing polymeric materials. Science 277:1225–1232
6. Chen JT, Thomas EL, Ober CK, Hwang SS (1995) Zigzag morphology of a poly(styrene-b-hexyl isocyanate) rod-coil block copolymer. Macromolecules 28:1688–1697
7. Chen JT, Thomas EL, Ober CK, Mao G-P (1996) Self-assembled smectic phases in rod-coil block copolymers. Science 273:343–346
8. Schlaad H, Krasia T, Antonietti M (2004) Superhelices of poly[2-(acetoacetoxy)ethyl methacrylate]. J Am Chem Soc 126:11307–11310
9. Vonau F, Suhr D, Aubel D, Bouteiller L, Reiter G, Simon L (2005) Evolution of multilevel order in supramolecular assemblies. Phys Rev Lett 94:066103
10. Zhou Y, Hall CK, Karplus M (1996) First-order disorder-to-order transition in an isolated homopolymer model. Phys Rev Lett 77:2822–2825
11. Ludwigs S, Krausch G, Reiter G, Losik M, Antonietti M, Schlaad H (2005) Structure formation of polystyrene-block-poly(γ-benzyl-L-glutamate) in thin films. Macromolecules 38:7532–7535
12. Minich EA, Nowak AP, Deming TJ, Pochan DJ (2004) Rod–rod and rod–coil self-assembly and phase behavior of polypeptide diblock copolymers. Polymer 45:1951–1957
13. Schlaad H, Antonietti M (2003) Block copolymers with amino acid sequences: molecular chimeras of polypeptides and synthetic polymers. Eur Phys J E 10:17–23
14. Botiz I, Grozev N, Schlaad H, Reiter G (2008) The influence of protic non-solvents present in the environment on structure formation of poly(γ-benzyl-L-glutamate) in organic solvents. Soft Matter 4:993–1002
15. Losik M, Kubowicz S, Smarsly B, Schlaad H (2004) Solid-state structure of polypeptide-based rod-coil block copolymers: Folding of helices. Eur Phys J E 15:407–411
16. Schlaad H, Smarsly B, Below I (2006) Solid-state structure of polystyrene-block-poly (γ-benzyl-L-glutamate): helix folding vs stretching. Macromolecules 39:4631–4632
17. Hol WGJ, van Duijnen PT, Berendsen HJC (1979) The α-helix dipole and the properties of proteins. Nature 273:443–446
18. Kukula H, Schlaad H, Tauer K (2002) Linear and star-shaped polystyrene-block-poly(sodium glutamate)s as emulsifiers in the heterophase polymerization of styrene. Macromolecules 35:2538–2544
19. Sakamoto R (1984) Phase separation of poly(γ-benzyl-L-glutamate) to liquid crystal and isotropic solution in various helicogenic solvents. Coll Polym Sci 262:788–792
20. Wee EL, Miller WG (1971) Liquid crystal-isotropic phase equilibriums in the system poly (γ-benzyl α-L-glutamate)-methylformamide. J Phys Chem 75:1446–1452
21. Flory PJ (1956) Statistical thermodynamics of semi-flexible chain molecules. Proc R Soc Lond A234:60–73
22. Robinson C (1956) Liquid-crystalline structures in solutions of a polypeptide. Trans Faraday Soc 52:571–592
23. Watanabe J, Goto M, Nagase T (1987) Thermotropic polypeptides. 3. Investigation of cholesteric mesophase properties of poly(γ-benzyl-L-glutamate-co-γ-dodecyl-L-glutamates) by circular dichroic measurements. Macromolecules 20:298–304
24. Russo PS, Miller WG (1983) Coexistence of liquid crystalline phases in poly(γ-benzyl α,L-glutamate)-dimethylformamide. Macromolecules 16:1690–1693
25. He S-J, Lee C, Gido SP, Yu SM, Tirrell DA (1998) A twist grain boundary-like twisted smectic phase in monodisperse poly(γ-benzyl α,L-glutamate) produced by recombinant DNA techniques. Macromolecules 31:9387–9389
26. Watanabe J, Imai K, Uematsu I (1978) Light scattering studies of poly(γ-benzyl L-glutamate) solutions and films. Polym Bull 1:67–72
27. Toriumi H, Minakuchi S, Uematsu Y, Uematsu I (1980) Helical twisting power of poly(γ-benzyl-L-glutamate) liquid crystals in mixed solvents. Polym J 12:431–437

28. Uematsu I (1984) Polypeptide liquid crystals. Adv Polym Sci 59:37–73
29. Robinson C, Ward JC (1957) Liquid-crystalline structures in polypeptides. Nature 180: 1183–1184
30. Robinson C, Ward JC, Beevers RB (1958) Liquid crystalline structure in polypeptide solutions. Part 2. Discuss Faraday Soc 25:29–42
31. Hill A, Donald AM (1989) Phase behaviour of poly-(γ-benzyl-L-glutamate) in benzyl alcohol. Liq Cryst 6:93–110
32. Block H, Shaw CP (1992) Second-harmonic generation in poly(α-amino acid) and poly(isocyanate) films. Polymer 33:2459–2462
33. Oxtoby DW (1992) Homogeneous nucleation: theory and experiment. J Phys Condens Matter 4:7627–7650
34. Sear RP (2007) Nucleation: theory and applications to protein solutions and colloidal suspensions. J Phys Condens Matter 19:033101
35. Mohanty R, Bhandarkar S, Estrin J (1990) Kinetics of nucleation from aqueous solution. AIChE J 36:1536–1544
36. Nielsen AE (1969) Nucleation and growth of crystals at high supersaturation. Kristall und Technik 4:17–38
37. Russo PS, Miller WG (1984) On the nature of the poly(γ-benzyl glutamate)-dimethylformamide “complex phase”. Macromolecules 17:1324–1331
38. Brandrup J, Immergut EH (1989) Polymer handbook, 3rd edn. Wiley, Chichester